



Heriot-Watt University
Research Gateway

Kinematic analysis of a single-loop reconfigurable 7R mechanism with multiple operation modes

Citation for published version:

He, X, Kong, X, Chablat, D, Caro, S & Hao, G 2014, 'Kinematic analysis of a single-loop reconfigurable 7R mechanism with multiple operation modes', *Robotica*. <https://doi.org/10.1017/S0263574713001197>

Digital Object Identifier (DOI):

[10.1017/S0263574713001197](https://doi.org/10.1017/S0263574713001197)

Link:

[Link to publication record in Heriot-Watt Research Portal](#)

Document Version:

Publisher's PDF, also known as Version of record

Published In:

Robotica

General rights

Copyright for the publications made accessible via Heriot-Watt Research Portal is retained by the author(s) and / or other copyright owners and it is a condition of accessing these publications that users recognise and abide by the legal requirements associated with these rights.

Take down policy

Heriot-Watt University has made every reasonable effort to ensure that the content in Heriot-Watt Research Portal complies with UK legislation. If you believe that the public display of this file breaches copyright please contact open.access@hw.ac.uk providing details, and we will remove access to the work immediately and investigate your claim.

Additional services for **Robotica**:

Email alerts: [Click here](#)

Subscriptions: [Click here](#)

Commercial reprints: [Click here](#)

Terms of use : [Click here](#)



Kinematic analysis of a single-loop reconfigurable 7R mechanism with multiple operation modes

Xiuyun He, Xianwen Kong, Damien Chablat, Stéphane Caro and Guangbo Hao

Robotica / FirstView Article / July 2014, pp 1 - 18

DOI: 10.1017/S0263574713001197, Published online: 22 January 2014

Link to this article: http://journals.cambridge.org/abstract_S0263574713001197

How to cite this article:

Xiuyun He, Xianwen Kong, Damien Chablat, Stéphane Caro and Guangbo Hao Kinematic analysis of a single-loop reconfigurable 7R mechanism with multiple operation modes . Robotica, Available on CJO 2014 doi:10.1017/S0263574713001197

Request Permissions : [Click here](#)

Kinematic analysis of a single-loop reconfigurable 7R mechanism with multiple operation modes

Xiuyun He[†], Xianwen Kong^{†*}, Damien Chablat[‡],
Stéphane Caro[‡] and Guangbo Hao[§]

[†]*School of Engineering and Physical Sciences, Heriot-Watt University, Edinburgh EH14 4AS, UK*

[‡]*Institut de Recherche en Communications et en Cybernétique de Nantes (IRCCyN), Université Nantes Angers Le Mans, Nantes, France*

[§]*School of Engineering, University College Cork, Cork, Ireland*

(Accepted November 26, 2013)

SUMMARY

This paper presents a novel one-degree-of-freedom (1-DOF) single-loop reconfigurable 7R mechanism with multiple operation modes (SLR7RMMOM), composed of seven revolute (R) joints, via adding a revolute joint to the overconstrained Sarrus linkage. The SLR7RMMOM can switch from one operation mode to another without disconnection and reassembly, and is a non-overconstrained mechanism. The algorithm for the inverse kinematics of the serial 6R mechanism using kinematic mapping is adopted to deal with the kinematic analysis of the SLR7RMMOM. First, a numerical method is applied and an example is given to show that there are 13 sets of solutions for the SLR7RMMOM, corresponding to each input angle. Among these solutions, nine sets are real solutions, which are verified using both a computer-aided design (CAD) model and a prototype of the mechanism. Then an algebraic approach is also used to analyse the mechanism and same results are obtained as the numerical one. It is shown from both numerical and algebraic approaches that the SLR7RMMOM has three operation modes: a translational mode and two 1-DOF planar modes. The transitional configurations among the three modes are also identified.

KEYWORDS: Single-loop reconfigurable mechanism; Multiple operation modes; Kinematic analysis; Numerical method; Algebraic approach; Transitional configuration.

1. Introduction

Reconfigurable mechanisms (RMs), which can generate different operation modes to fulfil variable tasks based on a sole mechanism, have received increasing attention from researchers around the world. Different approaches have been proposed to design RMs generating multiple motion patterns. Several classes of RMs have been developed, such as modular reconfigurable mechanisms,^{1,2} metamorphic mechanisms,³ kinematotropic mechanisms,⁴ variable actuated mechanisms,⁵ and reconfigurable mechanisms with multiple operation modes.^{6–8}

This paper focuses on the RMs with multiple operation modes^{6–9} since this class of RMs can be reconfigured without disassembly and without increasing the number of actuators. One design approach has been proposed in refs. [6]–[8] for the synthesis of reconfigurable mechanisms with multiple operation modes, including single-loop reconfigurable mechanisms with multiple operation modes^{6,7} and multiple-loop reconfigurable mechanisms with multiple operation modes.⁸ An intuitive approach⁶ was proposed to construct a single-loop reconfigurable mechanism with multiple operation modes by combining two overconstrained mechanisms. Using this approach, Huang *et al.*⁷ proposed a spatial 7-link mechanism by combining a Bennett linkage and a RPRP linkage (R: revolute joint; P: prismatic joint) and revealed that the mechanism has three operation modes: 5R2P, Bennett and RPRP. Another design approach for constructing single-loop reconfigurable mechanisms with multiple

* Corresponding author. E-mail: X.Kong@hw.ac.uk

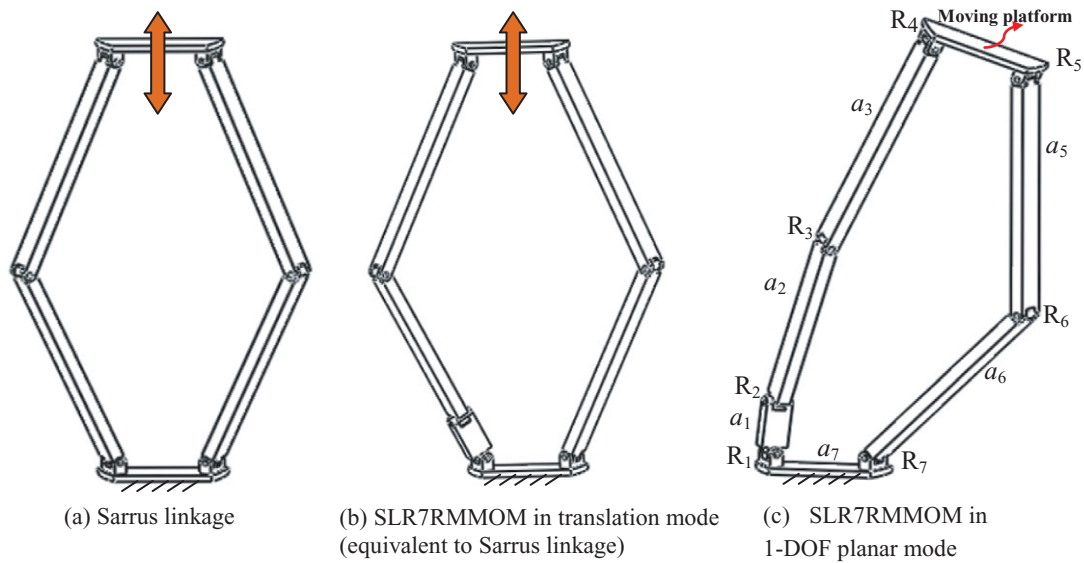


Fig. 1. (Colour online) Construction of the SLR7RMMOM.

operation modes is to insert one or more joints into an overconstrained mechanism.¹⁰ In this paper, we will propose a new 7R mechanism by inserting one R joint into the overconstrained Sarrus linkage. This mechanism has at least two operation modes: the Sarrus linkage motion mode (translational mode) and one planar mode. One apparent merit of the new 7R mechanism, compared to the original Sarrus linkage or other conventional single-mode 7R mechanisms, is that it has multiple operation modes.

Meanwhile, several analysis approaches have been developed to deal with the kinematics and singularity analysis of serial and parallel mechanisms, such as differential algorithm,¹¹ screw theory algorithm¹² and kinematic mapping algorithm.¹⁴ Husty and Pfurner have made a significant contribution to the kinematic mapping algorithm for the kinematic analysis of mechanisms.^{13–17} It has been shown that kinematic mapping algorithm is very efficient for both direct (forward) and inverse kinematic analysis of mechanisms.

The kinematic analysis of single-loop reconfigurable 7R mechanism with multiple operation modes (SLR7RMMOM) proposed in this paper is to be analysed using the effective algorithm for the inverse kinematics of a general serial 6R manipulator. The operation modes and transitional configurations will be identified. The paper is organised as follows. Section 2 describes one-degree-of-freedom (1-DOF) SLR7RMMOM. In Section 3, the kinematic analysis of the mechanism is undertaken within three steps mainly using the kinematic mapping method, and the solutions for a given input angle are verified using both a computer-aided design (CAD) model and a prototype. Based upon the results from Section 3, a series of input angles are given, and operation modes and transitional configurations are obtained in Section 4. In Section 5, algebraic approach is used to analyse the SLR7RMMOM again. Finally, conclusions are drawn.

2. Description of a 1-DOF SLR7RMMOM

It is well known that the Sarrus linkage (Fig. 1(a)), which is composed of two groups of three R joints with parallel joint axes (rotational axes), is used to control the 1-DOF translation of a moving platform along a straight line with respect to the base. Since the Sarrus linkage is an overconstrained mechanism, we can insert one additional R joint between the two joints of a link to obtain a new 1-DOF single-loop 7R mechanism (Fig. 1(b)).¹⁰ The advantages of adding one R joint to the Sarrus linkage are as follows: (a) it allows one to obtain a non-overconstrained mechanism from an overconstrained mechanism; (b) the Sarrus linkage has only one operation mode to complete one kind of task, but the new single-loop 7R mechanism has at least two operation modes with the possibility to fulfil different kinds of tasks on a sole mechanism; (c) the new single-loop 7R mechanism can switch

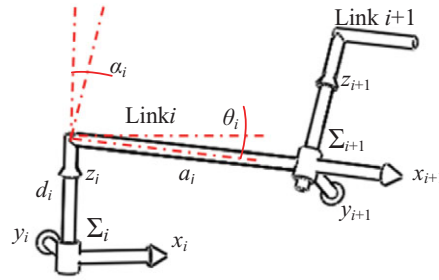


Fig. 2. (Colour online) D-H parameters (Σ is the coordinate frame system).

from one mode to another without disassembly and without adding other actuator to the mechanism. In the translational operation mode (Sarrus mode), it works as the Sarrus linkage, in which the moving platform translates along a straight line (Fig. 1(b)). In the 1-DOF planar operation mode, the moving platform undergoes a 1-DOF general planar motion (Fig. 1(c)). Therefore, the above 7R mechanism is an SLR7RMMOM which can switch from one operation mode to another without causing any disconnection, by using a break in transition configuration.

In this SLR7RMMOM, link 7 is the base and link 4 is specified as the moving platform. Links 4 and 7 are identical and the link lengths and the axes of the R joints satisfy the following conditions:

$$\mathbf{R}_1 // \mathbf{R}_3 // \mathbf{R}_4 \perp \mathbf{R}_2, \quad (1)$$

$$\mathbf{R}_5 // \mathbf{R}_6 // \mathbf{R}_7, \quad (2)$$

$$a_1 + a_2 = a_3 = a_5 = a_6, \quad (3)$$

where \mathbf{R}_i ($i = 1, 2, \dots, 7$) is the unit vector along the axis of joint R_i and a_i is the link length as indicated in Fig. 1(c).

Whether the SLR7RMMOM has additional operation modes except the two operation modes already known is unclear from only the construction of the mechanism. In Section 3, we will discuss the kinematic analysis of the SLR7RMMOM in order to identify all of its operation modes as well as transitional configurations that the mechanism can have while switching from one operation mode to another.

3. Kinematic Analysis and Numerical Example

Using the approach to the inverse kinematics for general 6R mechanism,^{13–15} one can perform the kinematic analysis of the SLR7RMMOM. Then all the operation modes and transition configurations of the mechanism can be identified.

3.1. D-H parameters for the mechanism

In order to define the transformation relations between the links, a coordinate frame Σ_i is attached to link i as follows: the z_i -axis coincides with the axis of joint R_i , the x_i -axis aligns with the common perpendicular to the z_{i-1} - and z_i -axes and the y_i -axis is defined by the right-hand rule. With this notation one could write the transformation matrix (\mathbf{T}_i) from Σ_i to Σ_{i+1} as

$$\mathbf{T}_i = \mathbf{M}_i \mathbf{G}_i = \begin{bmatrix} 1 & 0 & 0 & 0 \\ 0 & \cos(\theta_i) & -\sin(\theta_i) & 0 \\ 0 & \sin(\theta_i) & \cos(\theta_i) & 0 \\ 0 & 0 & 0 & 1 \end{bmatrix} \begin{bmatrix} 1 & 0 & 0 & 0 \\ a_i & 1 & 0 & 0 \\ 0 & 0 & \cos(\alpha_i) & -\sin(\alpha_i) \\ d_i & 0 & \sin(\alpha_i) & \cos(\alpha_i) \end{bmatrix}, \quad (4)$$

where θ_i and d_i are the revolute angle and distance between the two x -axes of links i and $i+1$, respectively, and α_i and a_i are the twist angle and distance between the two z -axes of links i and $i+1$, respectively (Fig. 2).

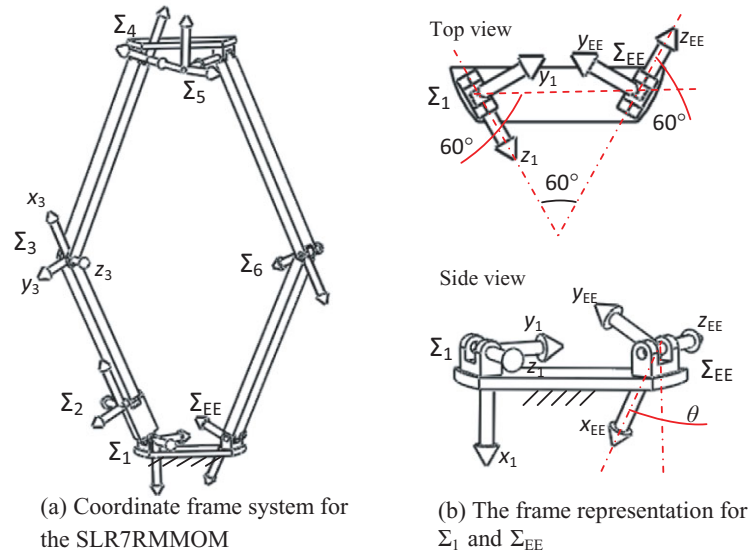


Fig. 3. (Colour online) Coordinate frame system for the SLR7RMMOM.

Table I. D-H parameters for the SLR7RMMOM.

i	a_i	d_i	α_i	θ_i
1	0.80	0	90°	θ_1
2	3.00	0	-90°	θ_2
3	3.80	0	0°	θ_3
4	0	1.47	-120°	θ_4
5	3.80	1.47	0°	θ_5
6	3.80	0	0°	θ_6

The SLR7RMMOM can be regarded as a 6R serial mechanism (Fig. 3(a)) with link 6 as the end-effector (EE), the coordinate frame on which is set as follows: its z -axis (z_{EE}) coincides with the axis of joint R_7 and its x -axis aligns with the common perpendicular to the z_6 -axis and the z_{EE} -axis. The angle between the x_{EE} -axis and the vertical line (θ) is defined as the input angle of the SLR7RMMOM (Fig. 3(b)). The D-H parameters of the 6R mechanism are shown in Table I, which should satisfy the conditions given in Section 2.

In addition, the angle between the axes of joints R_1 and R_7 is 60° , θ is specified as -45° and a_7 is 1.47 (note: throughout this paper, all rotational angles are defined to be positive if the rotation is in clockwise direction about the z -axis). Therefore, the pose of end-effector Σ_{EE} with respect to Σ_1 (A) can be obtained (Fig. 3(b)). First, the frame Σ_1 rotates 60° about the x -axis (R_1), then it translates 1.47 units along the z -axis (P_2) and rotates another 60° about its x -axis (R_3); finally we get the frame Σ_{EE} after rotating -45° about the z -axis (R_4):

$$A = R_1 \cdot P_2 \cdot R_3 \cdot R_4, \quad (5)$$

that is,

$$A = \begin{bmatrix} 1 & 0 & 0 & 0 \\ 0 & 0.7071067810 & 0.7071067810 & 0 \\ -1.273057344 & 0.3535533905 & -0.3535533905 & -0.8660254040 \\ 0.7350000000 & -0.6123724358 & 0.6123724358 & -0.5000000000 \end{bmatrix}.$$

3.2. Solutions of the kinematic analysis

The algorithm for the inverse kinematic analysis of a general 6R serial manipulator, presented in refs. [13]–[15], mainly used kinematic mapping method. Using this method, a Euclidean displacement can

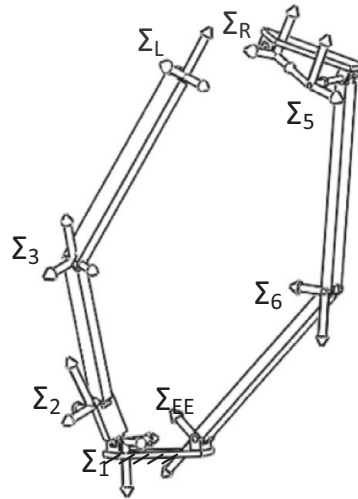


Fig. 4. Decomposing the 6R serial mechanism into two 3R chains.

be mapped into a point on a study quadric (S_6^2) in a seven-dimensional space, the so-called kinematic mapping space P^7 , where the point is displayed by eight study parameters. In the kinematic mapping space, the constraint manifold of a 2R chain is the intersection of a three-space with the S_6^2 and the constraint manifold of a 3R chain is the intersection of a set of three-spaces with the S_6^2 , where the set of three-spaces is called Segre Manifold (SM).¹³ The SM of a 3R chain can be represented by a set of four bilinear equations in the eight homogenous study parameters, which is denoted by z_0, z_1, \dots, z_7 , and one additional parameter corresponding to the tangent half of one joint angle out of the three joint angles. This means that there are three SMs ($SM_i, i = 1, 2, 3$) which are presented by three sets of four equations for a 3R chain.

The 6R serial mechanism associated with the 1-DOF SLR7RMMOM is further decomposed into two 3R chains, the left 3R one (1–2–3) with end effector frame Σ_L and the right 3R one (6–5–4) with end effector frame Σ_R (Fig. 4). The pose of the frame Σ_L with respect to Σ_1 (T_L) and the pose of the frame Σ_R with respect to Σ_1 (T_R) can be obtained based on Eqs. (4) and (5):

$$T_L = M_1 G_1 M_2 G_2 M_3 G_3, \quad (6a)$$

$$T_R = A G_6^{-1} M_6^{-1} G_5^{-1} M_5^{-1} G_4^{-1} M_4^{-1}. \quad (6b)$$

In the mechanism, the frames Σ_L and Σ_R have to coincide, which means that there is intersection among SM_L , SM_R and S_6^2 . The equations for the SMs can be derived from Eq. (6). Three sets of four equations can be obtained for the left or the right 3R chain, and each depends on one out of three joint angles.¹⁵ One needs to select one of the three sets of four equations for the left 3R chain and one of the three sets of four equations for the right 3R chain according to different situations¹⁵ before doing further calculation.

In some cases, not all the three SMs can be selected.¹⁵ If one selects one SM depending on one R joint with the joint axes of the remaining two parallel or intersected, in which case the SM lies on the S_6^2 , then the intersection of the SM with the S_6^2 fails. Therefore, we select SM_3 , which refers to four equations in v_3 (tangent half of θ_3), for the left 3R chain since the axes of joints R_1 and R_3 are parallel in the translational mode. For the right 3R chain, we select SM_5 with four equations in \bar{v}_5 (minus tangent half of θ_5), because the axes of joints R_4 and R_5 intersect and the axes of joints R_5 and R_6 are parallel. Thus eight equations for the 6R serial mechanism are obtained as follows:

$$h1_{v_3} : 30.4z_0 + 24.0z_1 + 6.4z_2v_3 - 8.0z_4 + 8.0z_5 - 8.0z_6v_3 - 8.0z_7v_3 = 0 \quad (7)$$

$$h2_{v_3} : 30.4z_0 - 24.0z_1 - 6.4z_2v_3 + 8.0z_4 + 8.0z_5 - 8.0z_6v_3 + 8.0z_7v_3 = 0 \quad (8)$$

$$h3_{v_3} : 6.4z_1v_3 - 24.0z_2 - 30.4z_3 - 8.0z_4v_3 + 8.0z_5v_3 + 8.0z_6 + 8.0z_7 = 0 \quad (9)$$

$$h4_{v_3} : -6.4z_1v_3 + 24.0z_2 + 30.4z_3 + 8.0z_4v_3 + 8.0z_5v_3 + 8.0z_6 - 8.0z_7 = 0 \quad (10)$$

$$\begin{aligned}
h5_{\bar{v}_5} : & z_0(2.72626795828513 - 6.58179306856969\bar{v}_5) + z_1(4.12012622455083 \\
& - 4.85463523903963\bar{v}_5) + z_2(8.65463523574647 - 5.69413776088330\bar{v}_5) \\
& + z_3(-1.37687417023358^{-9} + 4.47457271235407^{-9}\bar{v}_5) + z_4(1.24264068742686 \\
& - 3.00000000128678\bar{v}_5) + z_5(0.717438935080522 + 1.73205080649897\bar{v}_5) \\
& + z_6(1.73205080649897 - 0.717438935080522\bar{v}_5) + z_7(3.00000000128678 \\
& - 1.24264068742628\bar{v}_5) = 0
\end{aligned} \tag{11}$$

$$\begin{aligned}
h6_{\bar{v}_5} : & z_0(-2.7262679415240 + 6.58179306736930\bar{v}_5) + z_1(0.972103152392334 \\
& + 2.74536476831045\bar{v}_5) + z_2(8.65463523588648 + 5.69413776432743\bar{v}_5) \\
& + z_3(3.07322256531961^{-9} + 1.01209529645985^{-9}\bar{v}_5) + z_4(-0.414213562192757 \\
& - 0.99999999133379\bar{v}_5) + z_5(-0.717438935213303 - 1.73205080788068\bar{v}_5) \\
& + z_6(1.73205080788068 - 0.717438935213303\bar{v}_5) + z_7(-0.99999999133379 \\
& + 0.414213562192757\bar{v}_5) = 0
\end{aligned} \tag{12}$$

$$\begin{aligned}
h7_{\bar{v}_5} : & z_0(1.37687550250121^{-9} - 4.47457315644328^{-9}\bar{v}_5) + z_1(-8.65463523574647 \\
& - 5.69413776088330\bar{v}_5) + z_2(-4.12012622455083 + 4.85463523903963\bar{v}_5) \\
& + z_3(2.72626795828513 - 6.58179306856969\bar{v}_5) + z_4(-3.00000000128678 \\
& + 1.24264068742628\bar{v}_5) + z_5(1.73205080649897 - 0.717438935080522\bar{v}_5) \\
& + z_6(-0.717438935080522 - 1.73205080649897\bar{v}_5) + z_7(-1.24264068742686 \\
& - 3.00000000128678\bar{v}_5) = 0
\end{aligned} \tag{13}$$

$$\begin{aligned}
h8_{\bar{v}_5} : & z_0(-3.07322167714119^{-9} + 1.01209551850445^{-9}\bar{v}_5) + z_1(8.65463523588648 \\
& + 5.69413776432743\bar{v}_5) + z_2(0.972103152392334 - 2.74536476831045\bar{v}_5) \\
& + z_3(2.7262679415240 + 6.58179306736930\bar{v}_5) + z_4(0.99999999133379 \\
& - 0.414213562192757\bar{v}_5) + z_5(1.73205080788068 - 0.717438935213303\bar{v}_5) \\
& + z_6(0.717438935213303 + 1.73205080788068\bar{v}_5) + z_7(-0.414213562192757 \\
& - 0.99999999133379\bar{v}_5) = 0
\end{aligned} \tag{14}$$

$$h9 : z_0z_4 + z_1z_5 + z_2z_6 + z_3z_7 = 0 \tag{15}$$

Including the equation for the S_6^2 shown in Eq. (15), we obtain nine bilinear equations in 10 unknowns (Eqs. (7)–(15)). Because z_0, z_1, \dots , and z_7 are homogeneous, one of them can be normalised to 1. Solving seven of the nine equations to get the eight study parameters for z_0, z_1, \dots, z_7 in v_3 and \bar{v}_5 , and substituting the solutions into the remaining two equations, we obtain two equations in v_3 and \bar{v}_5 , named $E1$ and $E2$, as

$$\begin{aligned}
E1 : & v_3^4 \bar{v}_5^4 + 3.640783761v_3^4 \bar{v}_5^3 - 3.788653411v_3^3 \bar{v}_5^4 - 7.000053530v_3^4 \bar{v}_5^2 + 10.71593007v_3^3 \bar{v}_5^3 \\
& + 41.87086614v_3^2 \bar{v}_5^4 + 3.640783761v_3^4 \bar{v}_5 - 19.64341956v_3^2 \bar{v}_5^3 - 3.788653411v_3 \bar{v}_5^4 \\
& - 0.5952224873v_3^4 - 10.71593007v_3^4 \bar{v}_5 - 79.84271214v_3^2 \bar{v}_5^2 + 10.71593007v_3 \bar{v}_5^3 \\
& + 11.40205846\bar{v}_5^4 + 3.788653411v_3^3 - 19.64341956v_3^2 \bar{v}_5 - 23.28420332\bar{v}_5^3 \\
& + 53.83503480v_3^2 - 10.71593007v_3 \bar{v}_5 - 131.7802740\bar{v}_5^2 + 3.788653411v_3 \\
& - 23.28420332\bar{v}_5 + 24.96144960 = 0
\end{aligned} \tag{16}$$

$$\begin{aligned}
E2 : & v_3^8 \bar{v}_5^6 - 3.975059020v_3^8 \bar{v}_5^5 - 9.917459999v_3^7 \bar{v}_5^6 + 4.782767392v_3^8 \bar{v}_5^4 + 10.89653630v_3^7 \\
& - 7.905713714v_3^6 \bar{v}_5^6 - 2.187051780v_3^8 \bar{v}_5^3 + 10.76914366v_3^7 \bar{v}_5^4 + 11.58607438v_3^6 \bar{v}_5^5
\end{aligned}$$

$$\begin{aligned}
& -1.756500002v_3^5\bar{v}_5^6 + 0.1775892990v_3^8\bar{v}_5^2 - 6.718456391v_3^8 - 19.63855979v_3^6\bar{v}_5^4 \\
& - 3.599595703v_3^5\bar{v}_5^5 + 5.541460022v_3^4\bar{v}_5^6 + 0.1309074494v_3^8\bar{v}_5 - 10.68103759v_3^7\bar{v}_5^2 \\
& + 29.42980884v_3^6\bar{v}_5^3 + 88.38390043v_3^5\bar{v}_5^4 + 14.52156887v_3^4\bar{v}_5^5 - 11.11952017v_3^4\bar{v}_5^6 \\
& - 0.02663720154v_3^8 + 8.366957525v_3^7\bar{v}_5 + 1.744100557v_3^6\bar{v}_5^2 - 11.42375341v_3^5\bar{v}_5^3 \\
& + 47.03555747v_3^4\bar{v}_5^4 + 27.82871185v_3^3\bar{v}_5^5 + 23.16294757v_3^2\bar{v}_5^6 - 1.555454321v_3^7 \\
& - 14.97543807v_3\bar{v}_5^6 - 65.86121591v_3^5\bar{v}_5^2 + 22.54006617v_3^4\bar{v}_5^3 + 85.76873039v_3^3\bar{v}_5^4 \\
& - 19.01000389v_3^2\bar{v}_5^5 - 19.28048017v_3\bar{v}_5^6 + 4.289038591v_3^6 - 39.78294461v_3^5\bar{v}_5 \\
& - 55.12245682v_3^4\bar{v}_5^2 - 45.28245200v_3^3\bar{v}_5^3 + 12.06466530v_3^2\bar{v}_5^4 + 42.32484385v_3\bar{v}_5^5 \\
& + 8.715773829\bar{v}_5^6 - 4.399164900v_3^5 - 61.91885268v_3^4\bar{v}_5 - 206.5453764v_3^3\bar{v}_5^2 \\
& - 104.7180132v_3^2\bar{v}_5^3 + 8.153973623v_3\bar{v}_5^4 - 17.97043737\bar{v}_5^5 + 7.841437590v_3^4 \\
& - 127.7979408v_3^3v_3 - 166.3482520v_3^2\bar{v}_5^2 - 40.57715498v_3\bar{v}_5^3 - 59.39221935\bar{v}_5^4 \\
& - 2.488637296v_3^3 - 46.57694731v_3^2\bar{v}_5 - 151.3651980v_3\bar{v}_5^2 - 95.64121876\bar{v}_5^3 \\
& + 8.367254171v_3^3 - 79.64803864v_3\bar{v}_5 - 109.6592839\bar{v}_5^2 + 0.3550732836v_3 \\
& + 0.2355598536\bar{v}_5 + 4.481492373 = 0
\end{aligned} \tag{17}$$

Using the “resultant” command in Maple to eliminate \bar{v}_5 from Eqs. (16) and (17), one polynomial equation of degree 56 in v_3 named E can be derived as follows:

$$\begin{aligned}
E : (v_3^2 + 1)^6 (3.033362327v_3^4 - 12.05533640v_3^2 + 10.67784416) (1.87522003v_3^4 \\
- 64.00268390v_3^2 - 387.9596900)(5.157957061 \times 10^9v_3^{10} + 1.823061353 \times 10^{20}v_3^9 \\
- 7.297142808 \times 10^{21}v_3^8 + 1.634647033 \times 10^{22}v_3^7 + 5.885504960 \times 10^{22}v_3^6 \\
- 3.150969451 \times 10^{22}v_3^5 - 2.671416502 \times 10^{23}v_3^4 - 2.874236074 \times 10^{22}v_3^3 \\
+ 1.076318546 \times 10^{23}v_3^2 + 1.893149796 \times 10^{22}v_3 + 1.422425962 \times 10^{23})^2(6.60154501 \\
\times 10^8v_3^{16} + 2.698070325 \times 10^{18}v_3^{15} - 3.778024642 \times 10^{28}v_3^{14} - 8.52528086 \times 10^{37}v_3^{13} \\
+ 6.145569255 \times 10^{47}v_3^{12} - 4.007107158 \times 10^{49}v_3^{11} + 2.109260812 \times 10^{50}v_3^{10} \\
+ 3.306274920 \times 10^{49}v_3^9 + 5.471487282 \times 10^{50}v_3^8 + 1.795904346 \times 10^{51}v_3^7 - 1.709576046 \\
\times 10^{50}v_3^6 - 2.604353812 \times 10^{50}v_3^5 - 8.358864852 \times 10^{50}v_3^4 - 1.755833276 \times 10^{51}v_3^3 \\
+ 2.679828670 \times 10^{50}v_3^2 + 2.273726304 \times 10^5v_3 - 1.982814399 \times 10^{49}) = 0
\end{aligned} \tag{18}$$

The solutions to $(v_3^2 + 1)^6 = 0$ are $v_3 = \pm I$ (I is the unit imaginary number). The corresponding points in P^7 lie on the exceptional generator, which have to be cut out of the S_6^2 . The solutions of polynomial of 10 degrees squared are points with coordinate $(0, 0, 0, 0, 0, 0, 0)$, which do not lie on the S_6^2 and the solutions of polynomials of degree 4 are points that lie on the exceptional three-space of the S_6^2 .¹⁵ Then the polynomial of degree 16 gives the following 16 solutions:

$$\begin{aligned}
v_3 = [0.08366283786, 0.3610109062, 1.000000000, 6.521970015, 59.40599134, 4.132441204 \\
\times 10^9, 5.081725257 \times 10^9, 0.4234204659 + 2.169839731I, -0.07511185210 \\
+ 1.019253419I, -6.650597562 \times 10^9 + 3.156689159 \times 10^8I, -0.3581658035, \\
- 1.000000001, -1.507896627, -6.650597562 \times 10^9 - 3.156689159 \times 10^8I, \\
- 0.07511185210 - 1.019253419I, 0.4234204659 - 2.169839731I]
\end{aligned} \tag{19}$$

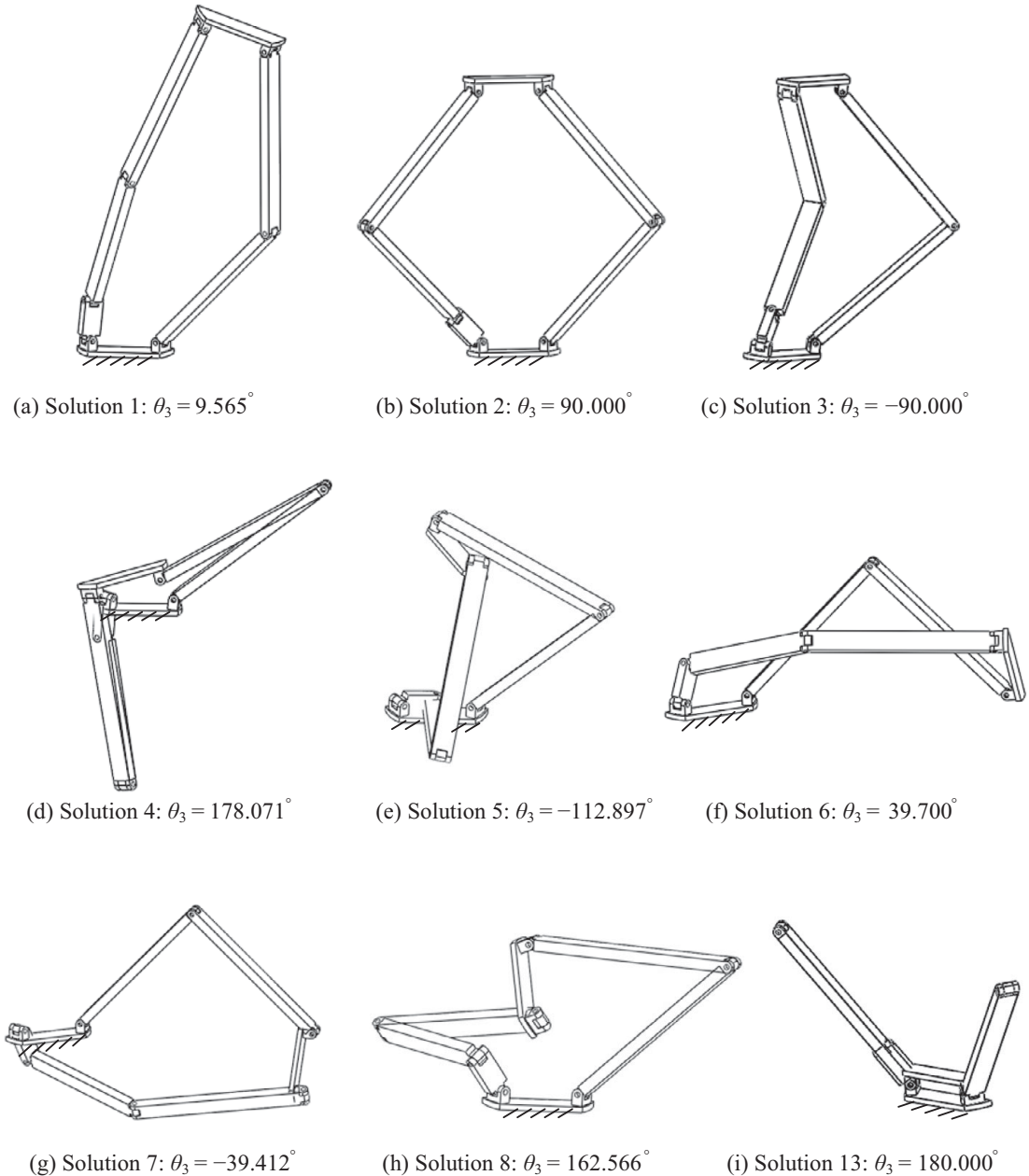


Fig. 5. CAD configurations corresponding to the real solutions for the SLR7RMMOM (Case $\theta = -45^\circ$).

Then the solutions for v_3 (Eq. (19)) are substituted back to $E1$ and $E2$, the common solutions for \bar{v}_5 with their corresponding v_3 are the solutions as desired. Please note only 12 sets of solutions could be easily obtained where the remaining four solutions for v_3 tend to be infinite, such as 5.081725257×10^9 and θ_3 approaches 180° . The remaining four joint angles for the normal 12 sets of solutions could be solved by the other sets of four equations for SM_1 , SM_2 , SM_4 and SM_6 .

As to the above four particular configurations, in which v_3 tends to infinite, there is one set of real solutions: any value of $\theta_1, \theta_2 = 0^\circ$, $\theta_3 = 180^\circ$, $\theta_4 = \theta_1 + 180$ (or $\theta_4 = \theta_1 - 180$), $\theta_5 = \theta = -45^\circ$ and $\theta_6 = 180^\circ$. This set of solutions can be easily verified by observation as shown in Fig. 5(i). This configuration is singular since the joint axes on the platform and the base coincide and the mechanism has 2-DOF. For any given θ , $\theta_4 = \theta_1 + 180$ (or $\theta_4 = \theta_1 - 180$) can take any value.

The complex solutions associated with the remaining three particular configurations are omitted in this paper.

Finally, 13 sets of solutions for the kinematic analysis of the single loop are obtained, as listed in Table II.

The above real solutions for the kinematic analysis have been verified using the CAD models for the 1-DOF SLR7RMMOM. The CAD configurations associated with these solutions are shown in Fig. 5.

3.3. Building prototype

A physical prototype has been built to verify the real solutions obtained above. Figure 6 illustrates that different configurations of the prototype corresponding to the real solutions can be achieved. It is noted that some configuration cannot be continuously generated in practice because of the interference between the links, such as configurations (e) and (g) (Figs. 6(e) and 6(g)).

4. Operation Modes and Transitional Configurations

As the input angle θ changes, a series of solutions corresponding to different input angles can be obtained accordingly using the numerical method proposed before. Then via plotting the joint angles against the input angle, we illustrate the operation modes and transitional configurations of the 1-DOF SLR7RMMOM (Fig. 7). All the operation modes and transitional configurations of the mechanism can be obtained from the plotting of angles θ_1 and θ_3 against the input angle θ . Please note that the singular configuration in which the moving platform and base coincide (see Figs. 5(i) and 6(i)) is discarded in this section.

Figure 7 shows that there are two straight lines A and B and two closed curves C ($C_0-C_1-C_2-C_0$ in Fig. 7(a) or $C_0-C_1-C_2-C_3-C_4-C_0$ in Fig. 7(b)) and D ($D_0-D_1-D_2-D_3-D_4-D_0$) designating the operation modes. Lines A and B are associated with translation operation mode, while the closed curves C and D are associated with two 1-DOF planar operation modes separately. Therefore, the mechanism has three operation modes but not only two operation modes. This can be easily verified by comparing the straight lines and closed curves to their corresponding operation mode figures in Fig. 5. Line A corresponds to Fig. 5(b), Line B corresponds to Fig. 5(c), closed curve C corresponds to Fig. 5(a), and closed curve D corresponds to Fig. 5(g). The eight real solutions (solution Nos. 1–8 in Table II) for θ_3 (or θ_1) under $\theta = -45^\circ$ are also indicated by the corresponding solution numbers, 1, 2, ..., 8 with shaded background in Fig. 7. Among these eight solutions, solution no. 2, solution no. 3, solution nos. 1, 4 and 6 and solution nos. 5, 7 and 8 fall on line A, line B, curve C and curve D, respectively.

In the following, the transitional configurations between three operation modes are analysed. By comparing the two plotting figures, Figs. 7(a) and 7(b), two intersecting points TA and TB through which two operation modes pass in both the plotting figures are apparently observed, which represent the two transitional configurations (Fig. 8). The input angles corresponding to the transitional configurations are shown in Table III.

5. Algebraic Approach

In this section, the algebraic approach proposed in refs. [16] and [17] will be applied to figure out the operation modes and transitional configurations. Apparently, compared to the above numerical method (Section 4), the algebraic approach enables the operation modes to be represented algebraically.

Without specifying the input angle as shown in Section 3, we present the end-effector pose \mathbf{A} and the equations for SM_i directly in θ . Therefore nine equations in v_3 (tangent half of θ_3), \bar{v}_5 (minus tangent half of θ_5), v (tangent half of θ) and eight study parameters (Eqs. (7)–(15)) can be obtained. Two equations in v_3 , \bar{v}_5 and v instead of two equations in v_3 and \bar{v}_5 will be obtained after solving seven of the nine equations and substituting the solutions into the remaining two equations. Using the “resultant” function in Maple to eliminate \bar{v}_5 (or v_3), we get the bivariate polynomial in the input angle v and one of the remaining joint parameter v_3 (or \bar{v}_5). Beside some spurious factors, there are three factors corresponding to three operation modes. For example, the input-output equation in v_3 and v is

$$S \cdot M1 \cdot M2 \cdot M3 = 0, \quad (20)$$

where S is a spurious factor. $M1$ is the input-output relation corresponding to the translational mode, while $M2$ and $M3$ represent the two general planar modes (see the Appendix for the detailed expressions).

Table II. Solutions for the SLR7RMMOM (Case $\theta = -45^\circ$).

Solutions	θ_1 (deg)	θ_2 (deg)	θ_3 (deg)	θ_4 (deg)	θ_5 (deg)	θ_6 (deg)
Solution 1	-173.940	20.726	9.565	-3.504	-155.426	-45.598
Solution 2	135.000	0.000	90.000	-45.000	-135.000	-90.000
Solution 3	-135.000	0.000	-90.000	45.000	-135.000	-90.000
Solution 4	-4.576	15.737	178.071	-2.648	-70.339	-172.852
Solution 5	-78.354	118.963	-112.897	-145.457	86.692	-119.924
Solution 6	-154.651	73.117	39.700	-14.351	131.208	90.703
Solution 7	-25.162	72.737	-39.412	-165.750	-41.899	90.473
Solution 8	141.385	-94.455	162.566	158.819	156.631	-137.538
Solution 9	$-54.493 - 109.370I$	$163.879 + 10.798I$	$-106.507 - 186.806I$	$-127.985 + 77.436I$	$58.785 + 82.626I$	$-100.688 - 144.387I$
Solution 10	$-54.493 + 109.370I$	$163.879 - 10.798I$	$-106.507 + 186.806I$	$-127.985 - 77.436I$	$58.785 - 82.626I$	$-100.688 + 144.387I$
Solution 11	$93.401 + 63.964I$	$-142.300 + 1.679I$	$167.711 + 54.093I$	$105.690 + 9.871I$	$112.781 + 77.655I$	$-156.361 - 28.617I$
Solution 12	$93.401 - 63.964I$	$-142.300 - 1.679I$	$167.711 - 54.093I$	$105.690 - 9.871I$	$112.781 - 77.655I$	$-156.361 + 28.617I$
Solution 13	Any value	0.000	180.000	$\theta_1 + 180$ (or $\theta_1 - 180$)	-45	180.000

Note: I is the imaginary unit.

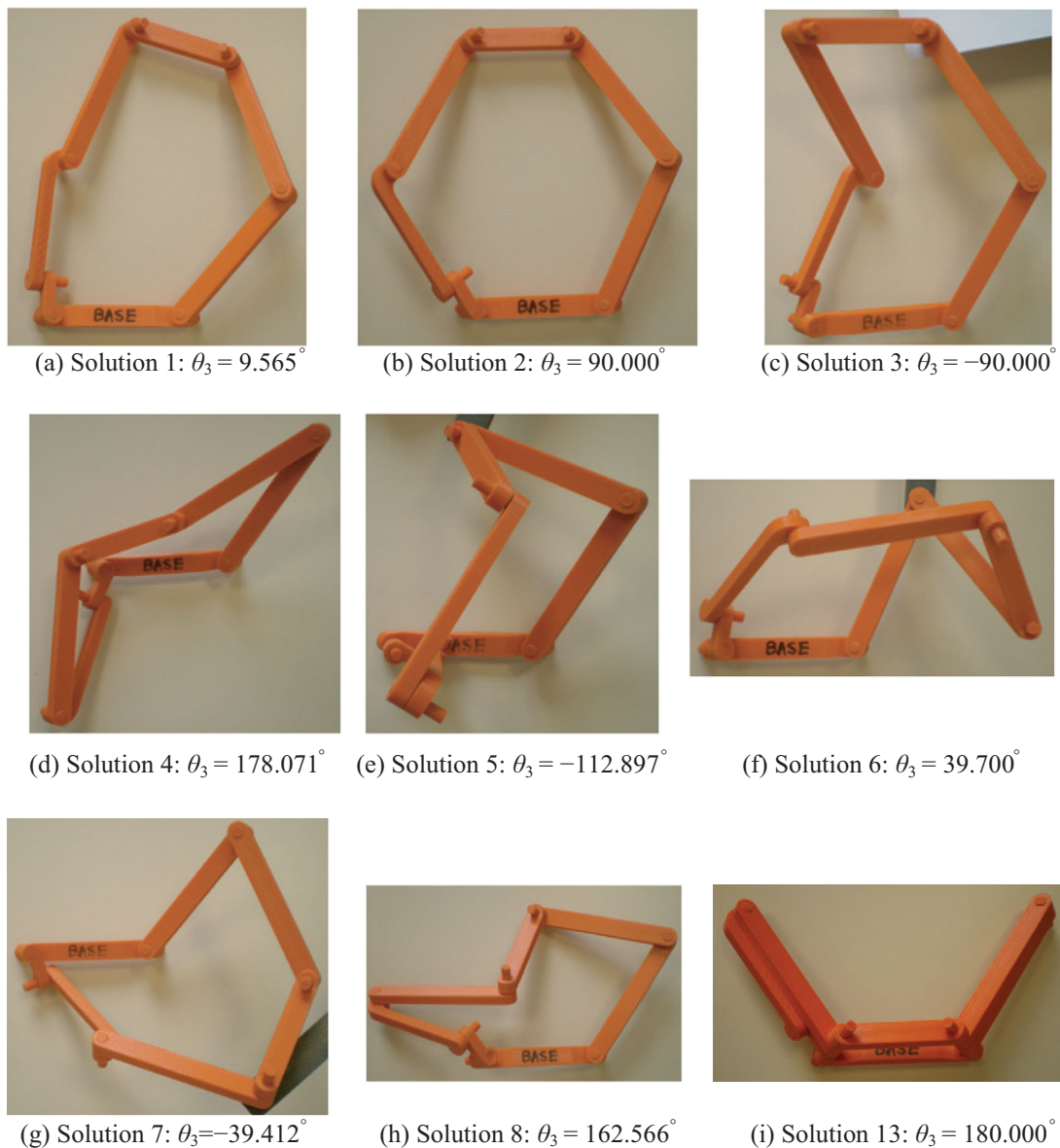


Fig. 6. (Colour online) Prototype configurations corresponding to the real solutions for the SLR7RMMOM (Case $\theta = -45^\circ$).

Table III. Transitional configurations.

Transition points	Input angle θ (deg)	Modes
TA	0	Translational mode & 1-DOF planar mode I (curve C)
TB	-180	Translational mode & 1-DOF planar mode II (curve D)

Then we can plot the input-output relation in v_3 and v (Fig. 9(a)), which shows three operation modes along with one transitional configuration. The solid curve corresponds to the translational mode, the dotted curve corresponds to the planar mode I and the dashed curve corresponds to planar mode II.

The numerical method is still kept in this paper even though it is not as simple or effective as the algebraic approach since it indicates all the results directly and clearly. The plots for the input-output angles in Fig. 7 show that there are two transitional configurations: (a) the input angle $\theta = 0^\circ$, the

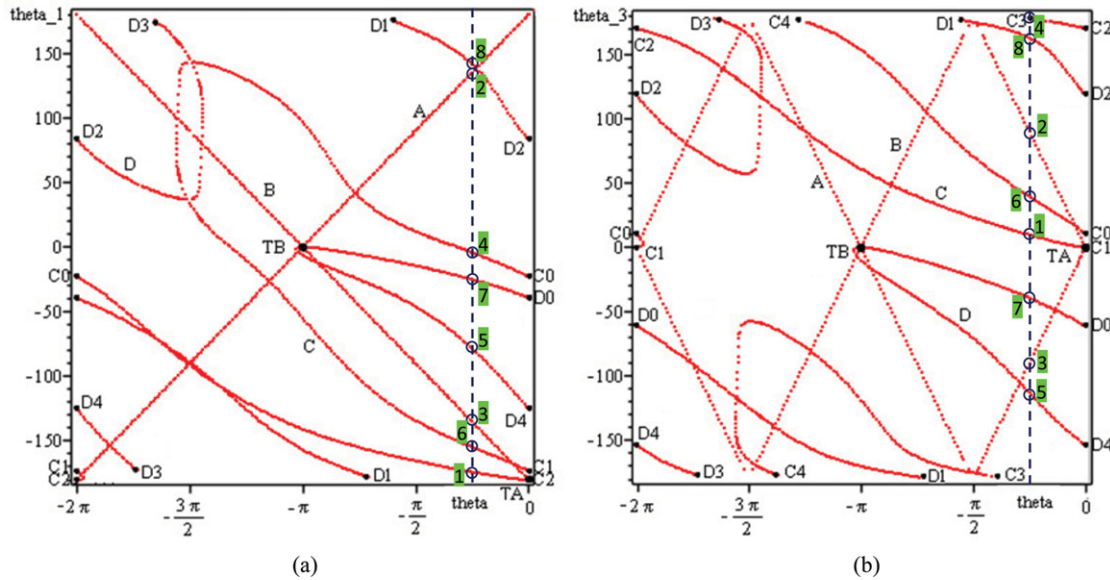


Fig. 7. (Colour online) Plotting of two rotational angles (θ_1 and θ_3) against input angle θ : (a) θ_1 (deg) in vertical axis versus θ (rad) in the horizontal axis; (b) θ_3 (deg) in vertical axis versus θ (rad) in the horizontal axis.

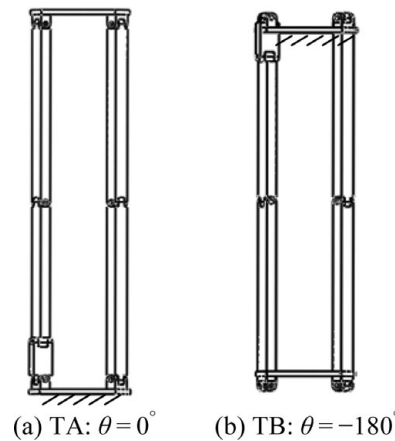


Fig. 8. Transitional configurations of the SLR7RMMOM.

revolute angles $\theta_3 = 0^\circ$ and $\theta_5 = 180^\circ$; (b) the input angle $\theta = -180^\circ$, the revolute angles $\theta_3 = 0^\circ$ and $\theta_5 = 0^\circ$. When the input angle $\theta = -180^\circ$, v tends to be infinite. Therefore the second transitional configuration cannot be seen directly from the plot of the input-output relation in v and v_3 (or v_5) in Fig. 9(a) using the algebraic approach. Then we have to use the reciprocal of variables to plot the relations in v and $1/v_5$, $1/v$ and v_3 as well as the relation in $1/v$ and v_5 (Fig. 9) so that all transitional configurations can be observed. In Fig. 9, the transition between the translation mode and planar mode I is TA, and the translation mode and planar mode II are transited at TB. It has been shown that the algebraic analysis results are the same as the numerical ones shown in Section 4 as expected.

6. Conclusions

This paper has presented a novel 1-DOF single-loop reconfigurable 7R mechanism with multiple operation modes (SLR7RMMOM) based on the Sarrus mechanism. The kinematic analysis of the novel SLR7RMMOM has been implemented using the algorithm for the inverse kinematics of a general serial 6R manipulator, which is very effective. Using a numerical method, a set of solutions for the 1-DOF SLR7RMMOM has been obtained for a given example and the real solutions have been verified through both the CAD model and the prototype of the mechanism. In addition, the numerical

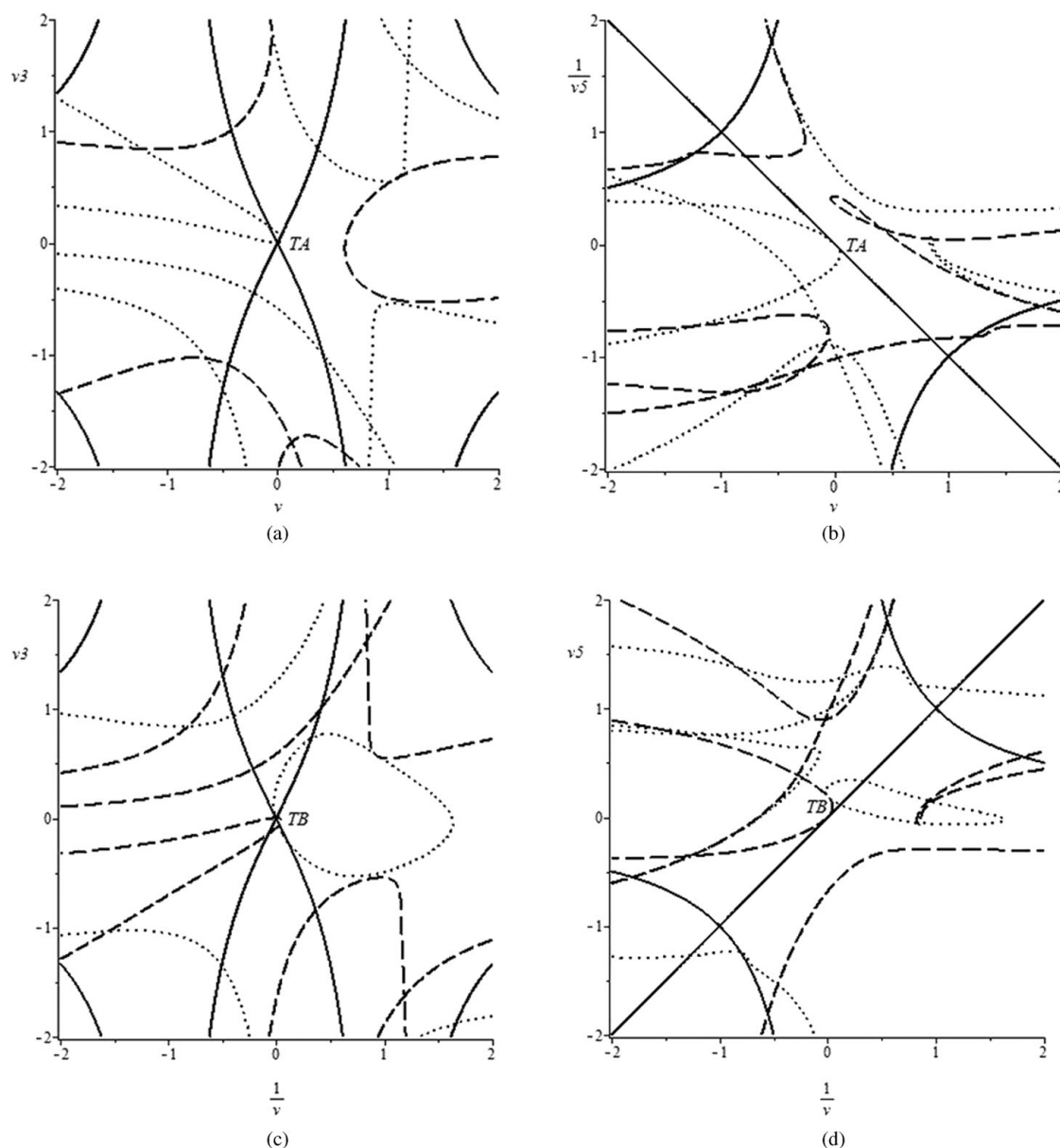


Fig. 9. Plots of the input-output equations using algebraic approach.

method and an algebraic approach have been used to obtain the operation modes and transitional configurations, which produce the same results. The mechanism has three operation modes: a translational mode and two 1-DOF planar modes, and there are two transitional configurations where the mechanism can switch from one operation mode to another.

The SLR7RMMOM on one hand is a non-overconstrained system and on the other hand can switch from one mode to another without disassembly and without using additional actuator, which can help develop energy-efficient reconfigurable mechanisms. The work proposed in this paper contributes to the design and analysis of new mechanical systems with multiple operation modes.

Acknowledgements

The authors would like to acknowledge the Royal Society, United Kingdom for the financial support through an International Joint Project No. JP100715. X. He would like to acknowledge the financial support from the SORSAS PhD scholarship in Heriot-Watt University. Special thanks go to Prof. M.

L. Husty and Dr. M. Pfurner in Universität Innsbruck, Austria for their valuable help in using their kinematic mapping algorithms.

References

1. G. Yang, I. Chen, K. M. Lim and Y. S. Huat, "Design and Kinematic Analysis of Modular Reconfigurable Parallel Robots," *Proceedings of the IEEE Conference on Robotics and Automation*, Detroit, MI, USA (May 1999) pp. 2501–2506.
2. G. Yang, I.-M. Chen, W. K. Lim and S. H. Yeo, "Kinematic design of modular reconfigurable in-parallel robots," *Auton. Robots* **10**(1), 83–89 (2001).
3. C. Kuo and J. Dai, "Reconfiguration Principles and Strategies for Reconfigurable Mechanisms," *ASME/IFToMM International Conference on Reconfigurable Mechanisms and Robots*, London, UK (Jun. 2009).
4. C. Galletti and P. Fanghella, "Single-loop kinematotropic mechanism," *Mech. Mach. Theory* **36**(6), 743–761 (2001).
5. N. Rakotomanga, D. Chablat and S. Caro, "Kinastatic Performance of a Planar Mechanism with Variable Actuation," *In: Advances in Robot Kinematics: Analysis and Design* (Springer, Netherlands, 2008) pp. 311–320.
6. X. Kong and C. Huang, "Type Synthesis of Single-DOF Single-Loop Mechanisms with Two Operation Modes," *ASME/IFToMM International Conference on Reconfigurable Mechanisms and Robots*, London, UK (Jun. 2009).
7. C. Huang, R. Tseng and X. Kong, "Design and Kinematic Analysis of a Multiple-Mode 5R2P Closed-Loop Linkage," *In: New Trends in Mechanism Science: Analysis and Design* (Springer, Netherlands, 2010) pp. 3–10.
8. X. Kong, "Type synthesis of 3-DOF parallel manipulators with both a planar operation mode and a spatial translational operation mode," *ASME J. Mech. Robot.* **5**(4), 041015 (2013).
9. D. Zlatanov, I. A. Bonev and C. M. Gosselin, "Constraint Singularity as C-space Singularities," *In: Advances in Robot Kinematics-Theory and Application* (Kluwer Academic Publishers, Netherlands, 2002) pp. 183–192.
10. X. Kong and C. M. Gosselin, *Type Synthesis of Parallel Mechanisms* (Springer, Netherlands, 2007).
11. X. Wang, M. Hao and Y. Cheng, "On the use of differential evolution for forward kinematics of parallel manipulators," *Appl. Math. Comput.* **205**(2), 760–769 (Nov. 2008).
12. I. A. Bonev, D. Zlatanov and C. M. Gosselin, "Singularity analysis of 3-DOF planar parallel mechanisms via screw theory," *ASME J. Mech. Des.* **125**(3), 573–581 (2003).
13. M. L. Husty, M. Pfurner and H. P. Schrocker, "A new and effective algorithm for the inverse kinematics of a general serial 6R manipulator," *Mech. Mach. Theory* **42**(1), 66–81 (2007).
14. M. L. Husty, M. Pfurner, H. P. Schrocker and K. Brunthaler, "Algebraic method in mechanism analysis and synthesis," *Robotica* **25**(6), 661–675 (2007).
15. M. Pfurner, *Analysis of Spatial Serial Manipulators Using Kinematic Mapping*, *PhD Thesis* (University of Innsbruck, Austria, 2006).
16. M. Pfurner, X. Kong, and C. Huang, "Algebraic Analysis of a Multiple-Mode 5R2P Closed-Loop Linkage," *Proceedings of International Line Geometry & Kinematics*, Paphos, Cyprus (Apr. 2011).
17. M. Pfurner, "Multiple-Mode Closed 7-Link Chains Based on Overconstrained 4-Link Mechanisms," *In: New Trends in Mechanism and Machine Science* (Springer, Netherlands, 2007) pp. 73–81.

Appendix: Expressions of $M1$, $M2$ and $M3$ in algebraic approach

$$\begin{aligned}
 M1 : & 5.14340728 \cdot 10^8 - 4.974625224 \cdot 10^{20} v v_3^2 + 3.729581608 \cdot 10^{21} v^2 v_3^2 \\
 & - 1.492387569 \cdot 10^{21} v^3 v_3^2 + 5.965621960 \cdot 10^{30} v^4 v_3^2 + 3.716176112 \cdot 10^{11} v^6 v_3^4 \\
 & + 4.858452837 \cdot 10^{11} v^4 v_3^4 - 1.492387569 \cdot 10^{21} v^5 v_3^2 + 3.729581608 \cdot 10^{21} v^6 v_3^2 \\
 & - 4.286183942 \cdot 10^{11} v^5 v_3^4 + 3.716176112 \cdot 10^{11} v^2 v_3^4 - 4.974625224 \cdot 10^{20} v^7 v_3^2 \\
 & + 1.176152683 \cdot 10^{11} v v_3^4 - 4.286183942 \cdot 10^{11} v^3 v_3^4 + 5.14340728 \cdot 10^8 v^8 \\
 & + 1.193124390 \cdot 10^{31} v^2 - 1.492387568 \cdot 10^{21} v^3 - 2.982810976 \cdot 10^{30} v_3^2 \\
 & + 9.856286305 \cdot 10^9 v_3^4 - 1.492387568 \cdot 10^{21} v^5 + 2.386248781 \cdot 10^{31} v^4 \\
 & + 1.193124390 \cdot 10^{31} v^6 - 4.974625226 \cdot 10^{20} v - 4.974625226 \cdot 10^{20} v^7 \\
 & + 9.856286305 \cdot 10^9 v^8 v_3^4 - 2.982810976 \cdot 10^{30} v^8 v_3^2 + 1.176152683 \cdot 10^{11} v^7 v_3^4 \quad (A.1)
 \end{aligned}$$

$$\begin{aligned}
M2 : & -2.729093868 \cdot 10^{23} v_3^4 - 8.219725596 \cdot 10^{22} v^4 v_3 - 9.415309985 \cdot 10^{22} v^5 v_3 \\
& - 1.563227815 \cdot 10^{24} v^6 v_3^2 + 1.296609173 \cdot 10^{23} v^2 v_3^4 - 7.332677035 \cdot 10^{23} v^4 v_3^2 \\
& - 3.317711885 \cdot 10^{23} v^5 v_3^3 - 6.304446700 \cdot 10^{22} v^4 v_3^3 - 9.350993671 \cdot 10^{23} v^5 v_3^4 \\
& + 4.705010277 \cdot 10^{23} v^4 v_3^4 + 1.029431363 \cdot 10^{24} v^6 v_3^4 - 3.013000688 \cdot 10^{22} v^2 v_3^3 \\
& - 7.746981730 \cdot 10^{23} v^5 v_3^2 - 9.407343642 \cdot 10^{19} v^6 v_3^3 - 2.245548577 \cdot 10^{23} v^{16} v_3^2 \\
& + 1.601045900 \cdot 10^{10} v^{17} v_3^{10} + 1.671978220 \cdot 10^{21} v^{18} v_3^4 + 6.949085491 \cdot 10^{22} v^{16} v_3^3 \\
& - 2.015199031 \cdot 10^{23} v^2 v_3^2 - 4.179048701 \cdot 10^{22} v^3 v_3 - 7.426364984 \cdot 10^{21} v v_3 \\
& - 3.778545211 \cdot 10^{22} v^2 v_3 - 1.291751125 \cdot 10^{23} v^3 v_3^3 - 2.130135835 \cdot 10^{22} v v_3^3 \\
& - 1.114703942 \cdot 10^{21} v^{17} v_3^6 + 3.021460303 \cdot 10^{22} v^6 v_3^8 + 9.497362709 \cdot 10^{22} v^7 v_3^7 \\
& - 2.906182293 \cdot 10^{23} v^8 v_3^6 + 3.631406041 \cdot 10^{20} v^{17} v_3^5 + 1.391713069 \cdot 10^{22} v^{16} v_3^5 \\
& - 4.509679151 \cdot 10^{10} v^{14} v_3^{10} - 6.610588067 \cdot 10^{20} v^{14} v_3^9 + 1.430990542 \cdot 10^{22} v^{16} v_3^6 \\
& + 3.237636303 \cdot 10^{21} v^{17} v_3^3 - 7.120464970 \cdot 10^{20} v^{16} v_3^7 + 1.267069468 \cdot 10^{22} v^{16} \\
& + 2.874684456 \cdot 10^{22} v^{17} + 2.116091480 \cdot 10^{20} v^{18} + 2.131332064 \cdot 10^{23} v^{15} \\
& - 5.012490592 \cdot 10^{19} v_3^9 + 2.739223748 \cdot 10^9 v_3^{10} + 3.395418194 \cdot 10^{21} v^{18} v_3^6 \\
& + 1.537105723 \cdot 10^{20} v^{18} v_3^7 - 2.353935684 \cdot 10^{20} v^{18} v_3^8 + 7.202206012 \cdot 10^{21} v^{18} v_3 \\
& + 3.231842146 \cdot 10^{23} v^{12} v_3 - 9.061650742 \cdot 10^{23} v^{11} v_3^2 - 8.451154603 \cdot 10^{22} v^8 v_3^5 \\
& + 3.492850997 \cdot 10^{23} v^7 v_3^6 - 1.236446233 \cdot 10^{23} v^6 v_3^7 - 3.666548230 \cdot 10^{22} v^5 v_3^8 \\
& + 3.396942214 \cdot 10^{22} v^{11} v_3 - 2.657235535 \cdot 10^{23} v^7 v_3^5 - 2.401407925 \cdot 10^{23} v^6 v_3^6 \\
& 4.855801959 \cdot 10^{21} v^{15} v_3^5 + 1.035323096 \cdot 10^{22} v^{15} v_3^6 + 3.682717202 \cdot 10^{21} v^{15} v_3^7 \\
& + 1.318474402 \cdot 10^{20} v^{17} v_3^9 - 2.584017612 \cdot 10^{23} v^3 v_3^2 - 3.717136071 \cdot 10^{22} v v_3^2 \\
& + 1.020247595 \cdot 10^{22} v^{15} v_3^8 + 1.872910691 \cdot 10^{22} v^{15} v_3 - 9.209535196 \cdot 10^{22} v^{15} v_3^2 \\
& + 8.956395465 \cdot 10^{21} v^{18} v_3^3 - 3.121087654 \cdot 10^{22} v^{18} v_3^2 - 4.202215811 \cdot 10^{22} v^{17} v_3^4 \\
& - 2.631478265 \cdot 10^{10} v^{16} v_3^{10} - 3.271580401 \cdot 10^{20} v^{16} v_3^9 + 3.065049286 \cdot 10^{21} v^{17} v_3 \\
& - 1.036711486 \cdot 10^{22} v^{17} v_3^2 + 1.793494749 \cdot 10^{21} v^{17} v_3^8 + 3.224010277 \cdot 10^{20} v^{17} v_3^7 \\
& + 1.077218029 \cdot 10^{22} v^{15} v_3^3 - 3.050778033 \cdot 10^{23} v^{15} v_3^4 + 1.537442313 \cdot 10^{21} v^{10} v_3^9 \\
& + 8.342942074 \cdot 10^{11} v^{10} v_3^{10} - 4.228619986 \cdot 10^{20} v^{11} v_3^9 + 5.235276346 \cdot 10^{10} v^3 v_3^{10} \\
& + 1.660389881 \cdot 10^{21} v_3^5 - 2.732015855 \cdot 10^{21} v_3^6 - 1.000695269 \cdot 10^{19} v_3^7 \\
& - 3.670260035 \cdot 10^{18} v_3^8 - 1.269214034 \cdot 10^{20} v^3 v_3^9 + 1.720991949 \cdot 10^{10} v^2 v_3^{10} \\
& - 2.523167259 \cdot 10^{20} v^2 v_3^9 + 1.406795912 \cdot 10^{10} v v_3^{10} + 1.376178294 \cdot 10^{19} v v_3^9 \\
& + 5.815925426 \cdot 10^{20} v^{15} v_3^9 + 1.484944730 \cdot 10^{10} v^{15} v_3^{10} + 4.587540209 \cdot 10^{22} v^{16} v_3^4 \\
& - 5.677910937 \cdot 10^{11} v^{11} v_3^{10} - 2.618407384 \cdot 10^{19} v^{12} v_3^9 + 2.625934822 \cdot 10^{11} v^{12} v_3^{10} \\
& - 2.558026327 \cdot 10^{22} v^{10} + 1.230036118 \cdot 10^{24} v^{11} - 3.775149946 \cdot 10^{23} v^{13} v_3^2 \\
& + 1.811095632 \cdot 10^{23} v^{14} v_3 + 3.188603172 \cdot 10^{22} v^8 v_3^8 + 9.598538192 \cdot 10^{22} v^9 v_3^7 \\
& - 2.027997927 \cdot 10^{23} v^{10} v_3^6 - 1.323983355 \cdot 10^{23} v^{11} v_3^5 + 8.011669620 \cdot 10^{23} v^{12} v_3^4 \\
& - 1.737196388 \cdot 10^{22} v^{13} v_3^3 - 7.450739151 \cdot 10^{23} v^{14} v_3^2 - 3.116986665 \cdot 10^{22} v^9 v_3^8
\end{aligned}$$

$$\begin{aligned}
& -1.320916071 \cdot 10^{23} v^{10} v_3^7 + 2.471985259 \cdot 10^{23} v^{11} v_3^6 + 3.864849903 \cdot 10^{22} v^{12} v_3^5 \\
& - 9.931611718 \cdot 10^{23} v^{13} v_3^4 + 2.314864589 \cdot 10^{23} v^{14} v_3^3 + 8.233479779 \cdot 10^{21} v^{10} v_3^8 \\
& + 6.824949120 \cdot 10^{23} v^{13} + 5.757483610 \cdot 10^{22} v^{11} v_3^7 - 6.491079126 \cdot 10^{22} v^{12} v_3^6 \\
& - 4.123656256 \cdot 10^{22} v^{13} v_3^5 + 2.769185526 \cdot 10^{23} v^{14} v_3^4 + 6.372648990 \cdot 10^{21} v^{11} v_3^8 \\
& - 5.968259264 \cdot 10^{22} v^{12} v_3^7 + 5.518883577 \cdot 10^{22} v^{16} v_3 - 3.618179662 \cdot 10^{21} v^{16} v_3^8 \\
& - 1.427931754 \cdot 10^{22} - 2.388161499 \cdot 10^{23} v^9 v_3^5 - 1.564266114 \cdot 10^{23} v^{11} v_3^3 \\
& - 1.529349097 \cdot 10^{24} v^{12} v_3^2 + 4.301113314 \cdot 10^{22} v^{13} v_3 - 5.229005887 \cdot 10^{22} v^7 v_3^8 \\
& + 7.345207896 \cdot 10^{20} v^{13} v_3^9 - 1.838966820 \cdot 10^{11} v^{13} v_3^{10} - 2.076061212 \cdot 10^{21} v^7 v_3^9 \\
& - 3.491945140 \cdot 10^{11} v^7 v_3^{10} + 1.988330841 \cdot 10^{21} v^8 v_3^9 + 9.682708067 \cdot 10^{11} v^8 v_3^{10} \\
& - 2.005703663 \cdot 10^{21} v^9 v_3^9 - 6.815067148 \cdot 10^{11} v^9 v_3^{10} - 2.320794093 \cdot 10^{20} v^4 v_3^9 \\
& + 1.372774005 \cdot 10^{11} v^4 v_3^{10} - 9.186784216 \cdot 10^{20} v^5 v_3^9 + 1.954373409 \cdot 10^{21} v^{18} v_3^5 \\
& - 4.647338417 \cdot 10^{19} v^{18} v_3^9 + 4.200143081 \cdot 10^9 v^{18} v_3^{10} - 1.445841816 \cdot 10^{10} v^5 v_3^{10} \\
& + 7.751910156 \cdot 10^{20} v^6 v_3^9 + 5.339586520 \cdot 10^{11} v^6 v_3^{10} - 4.326692914 \cdot 10^{22} v^6 v_3 \\
& - 1.308829187 \cdot 10^{24} v^7 v_3^2 - 3.496097199 \cdot 10^{22} v v_3^4 - 4.635391610 \cdot 10^{23} v^7 v_3^3 \\
& - 1.847512211 \cdot 10^{24} v^7 v_3^4 - 1.007659192 \cdot 10^{23} v^7 v_3 + 1.357352103 \cdot 10^{24} v^{10} v_3^4 \\
& + 4.357658036 \cdot 10^{23} v^{10} v_3^3 + 3.204970204 \cdot 10^{23} v^{10} v_3 - 3.711618302 \cdot 10^{23} v^9 v_3^3 \\
& - 1.365739731 \cdot 10^{24} v^9 v_3^2 + 1.378160493 \cdot 10^{23} v^8 v_3 - 3.435459472 \cdot 10^{22} v^9 v_3 \\
& - 2.199156271 \cdot 10^{24} v^8 v_3^2 - 2.169615058 \cdot 10^{24} v^{10} v_3^2 + 2.226642309 \cdot 10^{23} v^8 v_3^3 \\
& + 1.460796538 \cdot 10^{24} v^8 v_3^4 - 1.224281821 \cdot 10^{22} v^3 v_3^8 - 2.315631047 \cdot 10^{24} v^9 v_3^4 \\
& - 4.972961027 \cdot 10^{22} v^4 v_3^7 + 1.966909840 \cdot 10^{23} v^5 v_3^6 - 8.124695859 \cdot 10^{22} v^6 v_3^5 \\
& + 1.281356065 \cdot 10^{22} v^4 v_3^8 + 5.485095452 \cdot 10^{22} v^5 v_3^7 - 1.673713969 \cdot 10^{23} v^8 v_3^7 \\
& + 3.790788291 \cdot 10^{23} v^9 v_3^6 - 1.836026617 \cdot 10^{22} v^{10} v_3^5 - 1.895375315 \cdot 10^{24} v^{11} v_3^4 \\
& + 4.214891222 \cdot 10^{23} v^{12} v_3^3 + 8.648707732 \cdot 10^{22} v^{13} v_3^6 + 3.757043911 \cdot 10^{22} v^{14} v_3^5 \\
& - 1.300881573 \cdot 10^{22} v^{12} v_3^8 + 1.988105525 \cdot 10^{22} v^{13} v_3^7 + 9.245415773 \cdot 10^{21} v^{14} v_3^6 \\
& + 1.963834250 \cdot 10^{22} v^{13} v_3^8 - 1.346751537 \cdot 10^{22} v^{14} v_3^7 - 1.222933114 \cdot 10^{22} v^{14} v_3^8 \\
& - 1.176247323 \cdot 10^{22} v v_3^5 + 9.076241636 \cdot 10^{21} v v_3^6 - 5.478560916 \cdot 10^{20} v^2 v_3^5 \\
& + 2.126281914 \cdot 10^{21} v v_3^7 - 2.898900491 \cdot 10^{22} v^2 v_3^6 - 7.032280984 \cdot 10^{22} v^3 v_3^5 \\
& + 9.252874582 \cdot 10^{22} v^{12} + 6.017375655 \cdot 10^{22} v^{14} - 1.554240437 \cdot 10^{21} v v_3^8 \\
& - 8.455618050 \cdot 10^{21} v^2 v_3^7 + 6.338157158 \cdot 10^{22} v^3 v_3^6 - 3.034474190 \cdot 10^{22} v^4 v_3^5 \\
& + 2.085568621 \cdot 10^{21} v^2 v_3^8 + 1.693489424 \cdot 10^{22} v^3 v_3^7 - 1.153376251 \cdot 10^{23} v^4 v_3^6 \\
& - 1.818484557 \cdot 10^{23} v^5 v_3^5 - 6.235435335 \cdot 10^{21} v_3 - 2.431963915 \cdot 10^{22} v_3^2 \\
& + 9.013201546 \cdot 10^{22} v^3 - 4.615163407 \cdot 10^{21} v_3^3 - 9.708252461 \cdot 10^{22} v^2 \\
& - 2.712284396 \cdot 10^{23} v^4 - 3.880677938 \cdot 10^{23} v^6 + 1.669498494 \cdot 10^{22} v_3^4 \\
& + 3.937576605 \cdot 10^{23} v^5 + 8.420093360 \cdot 10^{21} v + 9.402581825 \cdot 10^{23} v^7 \\
& - 2.700368993 \cdot 10^{23} v^8 + 1.360140012 \cdot 10^{24} v^9
\end{aligned}
\tag{A.2}$$

$$\begin{aligned}
M3 : & 3.990045362 \cdot 10^{33} v_3^5 v_3^6 - 1.906546148 \cdot 10^{31} v_3^4 v_3^7 + 2.296394278 \cdot 10^{32} v_3^3 v_3^8 \\
& + 1.951298274 \cdot 10^{33} v_3^3 v_3^5 - 5.812123865 \cdot 10^{31} v_3^5 v_3^7 - 4.827086746 \cdot 10^{32} v_3^4 v_3^8 \\
& + 5.280010610 \cdot 10^{32} v_3^3 v_3^4 - 6.016597735 \cdot 10^{32} v_3^5 v_3 - 3.342554298 \cdot 10^{32} v_3^7 v_3 \\
& + 7.542872295 \cdot 10^{31} v_3^4 v_3 + 8.760836205 \cdot 10^{31} v_3^6 v_3 + 2.640005305 \cdot 10^{33} v_3^7 v_3^4 \\
& - 2.861873158 \cdot 10^{33} v_3^7 v_3^2 + 1.598539782 \cdot 10^{33} v_3^7 v_3^3 - 2.535198074 \cdot 10^{33} v_3^8 v_3^4 \\
& + 1.230826426 \cdot 10^{33} v_3^{10} v_3^3 + 3.314434734 \cdot 10^{33} v_3^{10} v_3^2 - 8.760836205 \cdot 10^{31} v_3^{10} v_3 \\
& - 1.976845023 \cdot 10^{33} v_3^{10} v_3^4 - 2.861873158 \cdot 10^{33} v_3^9 v_3^2 + 2.640005305 \cdot 10^{33} v_3^9 v_3^4 \\
& - 1.598539782 \cdot 10^{33} v_3^9 v_3^3 + 3.342554298 \cdot 10^{32} v_3^9 v_3 + 4.712020506 \cdot 10^{33} v_3^8 v_3^2 \\
& - 2.155613374 \cdot 10^{31} v_3^4 v_3 + 5.614836355 \cdot 10^{21} v_3^5 - 8.847937850 \cdot 10^{31} v_3^4 \\
& - 2.211984462 \cdot 10^{32} v_3^6 + 7.594963935 \cdot 10^{21} v_3^3 - 3.228957702 \cdot 10^{31} v_3^3 v_3^7 \\
& - 1.656517424 \cdot 10^{33} v_3^4 v_3^6 + 3.512336893 \cdot 10^{33} v_3^5 v_3^5 + 6.889182835 \cdot 10^{32} v_3^5 v_3^8 \\
& - 1.906546146 \cdot 10^{31} v_3^6 v_3^7 + 6.016597735 \cdot 10^{32} v_3^{11} v_3 + 1.951298274 \cdot 10^{33} v_3^7 v_3^5 \\
& - 5.188109825 \cdot 10^{33} v_3^6 v_3^6 - 8.791617325 \cdot 10^{31} v_3^3 v_3 - 1.474656308 \cdot 10^{31} v_3^2 \\
& + 8.760836210 \cdot 10^{31} v_3^4 v_3 + 3.314434734 \cdot 10^{33} v_3^6 v_3^2 + 2.877371606 \cdot 10^{33} v_3^5 v_3^3 \\
& + 9.744448600 \cdot 10^{32} v_3^4 v_3^2 - 2.237625055 \cdot 10^{32} v_3^2 v_3^4 - 1.230826426 \cdot 10^{33} v_3^4 v_3^3 \\
& + 1.584003182 \cdot 10^{33} v_3^5 v_3^4 - 9.114523580 \cdot 10^{32} v_3^4 v_3^4 - 1.976845023 \cdot 10^{33} v_3^6 v_3^4 \\
& - 1.717123895 \cdot 10^{33} v_3^5 v_3^2 - 1.230826426 \cdot 10^{33} v_3^6 v_3^3 + 3.197079563 \cdot 10^{32} v_3^3 v_3^3 \\
& - 5.274970395 \cdot 10^{32} v_3^2 v_3^3 + 1.598539782 \cdot 10^{33} v_3^3 v_3^3 + 3.754644091 \cdot 10^{31} v_3^2 v_3 \\
& - 6.685108595 \cdot 10^{31} v_3 v_3 - 3.342554298 \cdot 10^{32} v_3^3 v_3 - 8.176780455 \cdot 10^{31} v_3 v_3^2 \\
& - 5.723746320 \cdot 10^{32} v_3^3 v_3^2 - 4.671694796 \cdot 10^{31} v_3^2 v_3^2 - 6.273732740 \cdot 10^{31} v_3^2 \\
& + 3.990045362 \cdot 10^{33} v_3^{11} v_3^6 + 1.906546146 \cdot 10^{31} v_3^{10} v_3^7 - 6.453840515 \cdot 10^{31} v_3^2 v_3^8 \\
& - 1.360973320 \cdot 10^{33} v_3^4 v_3^5 + 1.330015120 \cdot 10^{33} v_3^3 v_3^6 - 8.170912070 \cdot 10^{30} v_3^2 v_3^7 \\
& + 3.280563254 \cdot 10^{31} v_3^8 v_3 - 1.360973320 \cdot 10^{33} v_3^6 v_3^5 - 3.597172912 \cdot 10^{20} \\
& - 9.114523580 \cdot 10^{32} v_3^{12} v_3^4 - 1.598539782 \cdot 10^{33} v_3^{13} v_3^3 - 4.671694796 \cdot 10^{31} v_3^{14} v_3^2 \\
& + 1.148197140 \cdot 10^{33} v_3^9 v_3^8 - 8.847937850 \cdot 10^{31} v_3^{12} + 6.257740155 \cdot 10^{30} v_3 \\
& - 2.684426957 \cdot 10^{31} v_3^2 v_3^6 - 6.457915405 \cdot 10^{30} v_3 v_3^7 - 5.832742800 \cdot 10^{32} v_3^2 v_3^5 \\
& - 9.374186485 \cdot 10^{10} v_3^6 v_3^{12} + 3.709352560 \cdot 10^{20} v_3^6 v_3^{11} + 5.229555090 \cdot 10^{30} v_3^6 v_3^{10} \\
& + 2.347307064 \cdot 10^{31} v_3^6 v_3^9 - 3.617136838 \cdot 10^{10} v_3^5 v_3^{12} - 8.905757360 \cdot 10^{19} v_3^5 v_3^{11} \\
& + 2.090922903 \cdot 10^{22} v_3^5 v_3^{10} - 9.142675110 \cdot 10^{31} v_3^5 v_3^9 + 2.554614344 \cdot 10^{10} v_3^4 v_3^{12} \\
& + 2.967482048 \cdot 10^{20} v_3^4 v_3^{11} + 1.034347964 \cdot 10^{30} v_3^4 v_3^{10} + 2.347307065 \cdot 10^{31} v_3^4 v_3^9 \\
& + 1.361436500 \cdot 10^{10} v_3^3 v_3^{12} - 4.947643038 \cdot 10^{19} v_3^3 v_3^{11} - 1.244643334 \cdot 10^{11} v_3^9 v_3^{12} \\
& + 4.947642948 \cdot 10^{19} v_3^9 v_3^{11} + 3.875811498 \cdot 10^{22} v_3^9 v_3^{10} + 5.079263950 \cdot 10^{31} v_3^9 v_3^9 \\
& + 3.280563254 \cdot 10^{31} v_3^{15} v_3^8 + 6.685108595 \cdot 10^{31} v_3^{15} v_3 - 8.176780455 \cdot 10^{31} v_3^{15} v_3^2 \\
& - 3.197079563 \cdot 10^{32} v_3^{15} v_3^3 + 7.542872295 \cdot 10^{31} v_3^{15} v_3^4 + 2.287889851 \cdot 10^{10} v_3^{14} v_3^{12} \\
& - 7.418705120 \cdot 10^{19} v_3^{14} v_3^{11} - 4.570575250 \cdot 10^{29} v_3^{14} v_3^{10} - 1.005988742 \cdot 10^{31} v_3^{14} v_3^9 \\
& + 6.23978001 \cdot 10^8 v_3^{12} - 5.333963550 \cdot 10^9 v_3^{11} - 1.888346556 \cdot 10^{29} v_3^{10}
\end{aligned}$$

$$\begin{aligned}
& + 1.676647904 \cdot 10^{30} v_3^9 + 2.311427381 \cdot 10^{21} v^{15} + 5.405983040 \cdot 10^{21} v^3 v_3^{10} \\
& - 5.079263950 \cdot 10^{31} v^3 v_3^9 - 3.597172912 \cdot 10^{20} v^{16} - 2.211984462 \cdot 10^{32} v^{10} \\
& - 2.949312616 \cdot 10^{32} v^8 - 4.950318962 \cdot 10^{21} v^9 - 9.721238000 \cdot 10^{31} v_3^5 \\
& + 7.477259030 \cdot 10^{31} v_3^6 - 1.361818680 \cdot 10^{30} v_3^7 + 4.773912180 \cdot 10^{30} v_3^8 \\
& + 5.614836355 \cdot 10^{21} v^{11} + 7.594963935 \cdot 10^{21} v^{13} + 2.287889851 \cdot 10^{10} v^2 v_3^{12} \\
& + 7.418705120 \cdot 10^{19} v^2 v_3^{11} - 4.570575250 \cdot 10^{29} v^2 v_3^{10} + 1.005988742 \cdot 10^{31} v^2 v_3^9 \\
& + 7.445942390 \cdot 10^9 v v_3^{12} - 9.895286260 \cdot 10^{18} v v_3^{11} + 4.371918688 \cdot 10^{20} v v_3^{10} \\
& - 1.015852790 \cdot 10^{31} v v_3^9 - 1.951298274 \cdot 10^{33} v^9 v_3^5 - 2.877371606 \cdot 10^{33} v^{11} v_3^3 \\
& + 9.744448600 \cdot 10^{32} v^{12} v_3^2 + 3.342554298 \cdot 10^{32} v^{13} v_3 + 1.148197140 \cdot 10^{33} v^7 v_3^8 \\
& + 6.650075605 \cdot 10^{33} v^9 v_3^6 + 1.360973320 \cdot 10^{33} v^{10} v_3^5 + 1.584003182 \cdot 10^{33} v^{11} v_3^4 \\
& + 1.230826426 \cdot 10^{33} v^{12} v_3^3 - 5.723746320 \cdot 10^{32} v^{13} v_3^2 - 3.754644091 \cdot 10^{31} v^{14} v_3 \\
& - 1.720420200 \cdot 10^{33} v^8 v_3^8 + 3.228957702 \cdot 10^{31} v^9 v_3^7 - 5.188109825 \cdot 10^{33} v^{10} v_3^6 \\
& - 3.512336893 \cdot 10^{33} v^{11} v_3^5 - 1.951298274 \cdot 10^{33} v^{13} v_3^5 - 1.656517424 \cdot 10^{33} v^{12} v_3^6 \\
& + 5.812123865 \cdot 10^{31} v^{11} v_3^7 - 1.273606457 \cdot 10^{33} v^{10} v_3^8 + 5.274970395 \cdot 10^{32} v^{14} v_3^3 \\
& + 5.280010610 \cdot 10^{32} v^{13} v_3^4 + 1.360973320 \cdot 10^{33} v^{12} v_3^5 - 1.940661756 \cdot 10^{11} v^8 v_3^{12} \\
& - 1.474656308 \cdot 10^{31} v^{14} - 8.760836210 \cdot 10^{31} v^{12} v_3 - 1.273606457 \cdot 10^{33} v^6 v_3^8 \\
& - 3.228957702 \cdot 10^{31} v^7 v_3^7 - 7.266418520 \cdot 10^{33} v^8 v_3^6 - 1.717123895 \cdot 10^{33} v^{11} v_3^2 \\
& + 6.650075605 \cdot 10^{33} v^7 v_3^6 + 1.900021600 \cdot 10^{32} v v_3^6 + 3.902596548 \cdot 10^{32} v v_3^5 \\
& - 6.453840515 \cdot 10^{31} v^{14} v_3^8 + 8.170912070 \cdot 10^{30} v^{14} v_3^7 + 2.296394278 \cdot 10^{32} v^{13} v_3^8 \\
& + 2.311427381 \cdot 10^{21} v - 4.950318962 \cdot 10^{21} v^7 - 2.684426957 \cdot 10^{31} v^{14} v_3^6 \\
& + 3.228957702 \cdot 10^{31} v^{13} v_3^7 - 4.827086746 \cdot 10^{32} v^{12} v_3^8 + 5.832742800 \cdot 10^{32} v^{14} v_3^5 \\
& + 1.330015120 \cdot 10^{33} v^{13} v_3^6 + 1.906546148 \cdot 10^{31} v^{12} v_3^7 + 6.889182835 \cdot 10^{32} v^{11} v_3^8 \\
& - 2.237625055 \cdot 10^{32} v^{14} v_3^4 + 7.853968510 \cdot 10^{30} v^8 v_3^{10} - 1.244643334 \cdot 10^{11} v^7 v_3^{12} \\
& - 4.947642948 \cdot 10^{19} v^7 v_3^{11} + 3.875811498 \cdot 10^{22} v^7 v_3^{10} - 5.079263950 \cdot 10^{31} v^7 v_3^9 \\
& + 1.361436500 \cdot 10^{10} v^{13} v_3^{12} + 4.947643038 \cdot 10^{19} v^{13} v_3^{11} + 5.405983040 \cdot 10^{21} v^{13} v_3^{10} \\
& + 5.079263950 \cdot 10^{31} v^{13} v_3^9 + 2.554614344 \cdot 10^{10} v^{12} v_3^{12} - 2.967482048 \cdot 10^{20} v^{12} v_3^{11} \\
& + 1.034347964 \cdot 10^{30} v^{12} v_3^{10} - 2.347307065 \cdot 10^{31} v^{12} v_3^9 - 3.617136838 \cdot 10^{10} v^{11} v_3^{12} \\
& + 8.905757360 \cdot 10^{19} v^{11} v_3^{11} + 2.090922903 \cdot 10^{22} v^{11} v_3^{10} + 9.142675110 \cdot 10^{31} v^{11} v_3^9 \\
& - 9.374186485 \cdot 10^{10} v^{10} v_3^{12} - 3.709352560 \cdot 10^{20} v^{10} v_3^{11} + 5.229555090 \cdot 10^{30} v^{10} v_3^{10} \\
& - 2.347307064 \cdot 10^{31} v^{10} v_3^9 + 6.23978001 \cdot 10^8 v^{16} v_3^{12} + 5.333963550 \cdot 10^9 v^{16} v_3^{11} \\
& - 1.888346556 \cdot 10^{29} v^{16} v_3^{10} - 1.676647904 \cdot 10^{30} v^{16} v_3^9 + 9.721238000 \cdot 10^{31} v^{16} v_3^5 \\
& + 7.477259030 \cdot 10^{31} v^{16} v_3^6 + 1.361818680 \cdot 10^{30} v^{16} v_3^7 + 4.773912180 \cdot 10^{30} v^{16} v_3^8 \\
& - 6.257740155 \cdot 10^{30} v^{16} v_3^3 - 6.273732740 \cdot 10^{31} v^{16} v_3^2 + 8.791617325 \cdot 10^{31} v^{16} v_3^3 \\
& - 2.155613374 \cdot 10^{31} v^{16} v_3^4 + 7.445942390 \cdot 10^9 v^{15} v_3^{12} + 9.895286260 \cdot 10^{18} v^{15} v_3^{11} \\
& + 4.371918688 \cdot 10^{20} v^{15} v_3^{10} + 1.015852790 \cdot 10^{31} v^{15} v_3^9 - 3.902596548 \cdot 10^{32} v^{15} v_3^5 \\
& + 1.900021600 \cdot 10^{32} v^{15} v_3^6 + 6.457915405 \cdot 10^{30} v^{15} v_3^7
\end{aligned} \tag{A.3}$$